Direct quantum dynamics using grid-based wavefunction propagation and machine-learned potential energy surfaces

Gareth W. Richings and Scott Habershon*

Department of Chemistry and Centre for Scientific Computing, University of Warwick, Coventry, CV4 7AL, United Kingdom

E-mail: S.Habershon@warwick.ac.uk

Abstract

We describe a method for performing nuclear quantum dynamics calculations using standard, grid-based algorithms, including the multi configurational time-dependent Hartree (MCTDH) method, where the potential energy surface (PES) is calculated "on-the-fly". The method of Gaussian process regression (GPR) is used to construct a global representation of the PES using values of the energy at points distributed in molecular configuration space during the course of the wavepacket propagation. We demonstrate this direct dynamics approach for both an analytical PES function describing 3-dimensional proton transfer dynamics in malonaldehyde, and for 2- and 6-dimensional quantum dynamics simulations of proton transfer in salicylaldimine. In the case of salicylaldimine we also perform calculations in which the PES is constructed using Hartree-Fock calculations through an interface to an *ab initio* electronic structure code. In all cases, the results of the quantum dynamics simulations are in excellent agreement with previous simulations of both systems, yet do not require prior fitting of a PES at any stage. Our approach (implemented in a development version of the *Quantics* package) opens a route to performing accurate quantum dynamics simulations *via* wavefunction propagation of many-dimensional molecular systems in a direct and efficient manner.

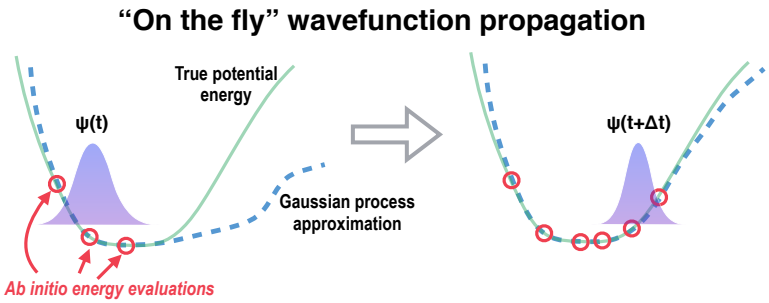

Table of contents (TOC) graphical abstract.

1 Introduction

The computer simulation of the dynamical behaviour of molecules is vital in providing understanding of processes which are important across chemistry, materials science and biology. Such simulations can be performed using methods based on classical mechanics, but many processes which are important in biological systems, for example proton transfer mechanisms in enzyme catalysis[1,2] or the photochemistry of DNA[3,4] and plant sunscreen molecules,[5,6] are fundamentally quantum mechanical in nature. It follows that simulation methods including the effects of quantum mechanics are needed to provide an accurate representation of the system being studied.

To model quantum molecular dynamics we must solve the time-dependent Schrödinger equation (TDSE) for nuclear motion,

$$i\hbar\frac{\partial\Psi\left(\mathbf{q},t\right)}{\partial t}=\hat{H}\Psi\left(\mathbf{q},t\right), \tag{1}$$

where $\{\mathbf{q}\}$ is the set of degrees-of-freedom (DOFs) of nuclear motion. Methods for following the time evolution of the wavefunction have been developed and refined over the past few decades, but among the most successful are those based on expanding the wavefunction in terms of a grid of basis functions localised in molecular configuration space. The method of choice in this field is the multi-configuration time-dependent Hartree (MCTDH) approach[7–13] which allows the treatment of systems of a few tens of DOFs and converges to the exact answer given a large enough basis set. Recently, so-called multi-layer MCTDH has been developed as an extension of the original method, allowing the description of the dynamics of systems with several hundred DOFs.[14–18]

The central difficulty of carrying out quantum dynamics calculations using grid-based methods is the need to define the form of the Hamiltonian operator, $\hat{H}$, prior to carrying out the wavepacket propagation. The nuclear wavefunction evolves on a potential energy surface (PES) defined by the solution of the electronic Schrödinger equation at points in

nuclear configuration space. As the wavefunction is a delocalised entity, the global form of the PES must be known in order to define the Hamiltonian. The fitting of some appropriate functional form to electronic energies is a common way of determining the PES, for example using the vibronic coupling Hamiltonian (VCHAM) method,[11,12,19,20] but this can be an arduous process if many nuclear DOFs and/or multiple electronic states are to be included in the Hamiltonian. The process can be simplified if a convenient choice of coordinate system is chosen to model the dynamics, but such a choice can often yield a kinetic energy operator with a complicated form.[21]

To overcome the problems associated with PES fitting and coodinate system choice, direct dynamics (DD) methods have been developed recently.[22,23] These approaches circumvent the long-winded PES fitting procedure by generating the PES during the course of the dynamics calculation. They avoid the global fitting of the PES by expanding the nuclear wavefunction in terms of basis functions of particular localised form which mean that only a localised knowledge of the potential around the centre of the functions is needed. This local representation also means that the choice of coordinate system is less important as there is no need to seek a simple global function to represent the PES, meaning that coordinate systems where the kinetic energy operator has a simple convenient form (*e.g.* Cartesian coordinates or normal modes) can be used. Among the most successful DD methods in use are the trajectory surface hopping (TSH)[24–42] and *ab initio* multiple spawning (AIMS)[43–47] methods which have both been used in studies on photochemistry in complex environments. The former method uses multiple classical trajectories to model the nuclear dynamics, with *ab initio* electronic energies being used to provide the forces along the trajectories. AIMS uses an expansion of the nuclear wavefunction in terms of Gaussian wavepackets, the centres of which evolve classically while the coefficients of the Gaussians in the wavefunction expansion are propagated quantum mechanically, with local approximations to the PES used to evaluate the associated matrix elements. Both methods can model the transfer of the wavefunction between multiple electronic states; TSH by allowing trajectories to hop be-

tween the states and AIMS by spawning new Gaussian functions on different states. A fully quantum mechanical DD method has also been implemented, based on the variational multi-configuration Gaussian (vMCG) method,[48,49] whereby, similar to AIMS, the wavefunction is represented by a linear combination of Gaussian wavepackets. The vMCG method, however, employs variational quantum evolution of both the Gaussian basis functions *and* the expansion coefficients. The DD-vMCG method[50–62] relies on using a Shepard interpolation of the PES to calculate the matrix elements required for propagation; the electronic energy, and its gradient and Hessian, are periodically evaluated at the centre of the Gaussian functions, and the local harmonic approximations to the PES that can then be formed around these points are combined in a weighted sum to give an approximate global PES. Despite their success, these three popular methods outlined each have issues which makes them less than ideal when used to model nuclear dynamics; TSH and AIMS rely on classical dynamics which makes them less able to model such features as tunnelling, while the fully quantum vMCG method suffers from numerical issues related to the use of a non-orthogonal basis of Gaussian functions (particularly relating to the linear dependence of the functions causing singularities in the equations-of-motion[50,63]).

Ideally a method is required which combines the stability and fully quantum nature of grid-based dynamics methods, such as MCTDH, with the ease of use and convenience of the DD methods described above. Although the DD-vMCG method uses an approximation to the full PES, the Shepard interpolation used is not suitable for MCTDH as it does not have the required sum-of-products form for efficient propagation of the MCTDH wavefunction. This desirable aspect of the PES for MCTDH will be considered more fully later but, briefly, it means that the PES is represented as a linear combination of functions which are products of separate terms in each DOF.

In this work, we present a new direct grid-based dynamics method based around the use of Gaussian Process Regression (GPR)[64–71] to expand the PES. The roots of this method lie within the field of Bayesian statistics, but the method can be used to generate a rep-

resentation of the PES based upon a linear expansion of Gaussian functions distributed across configuration space, yielding a PES in the sum-of-products form required for efficient MCTDH simulations. Here, we test this methodology in simulations of two molecules where intra-molecular proton transfer on the electronic ground state acts as a mechanism for tautomerisation, namely malonaldehyde[8–10,17,72–75] and salicylaldimine,[50,60,76] both of which are useful systems for study using quantum dynamics methods due to the role of tunnelling in the proton dynamics. This work complements a concurrent piece of work carried out by us, which demonstrated how a similar GPR-based methodology, combined with a propagated diabatisation scheme and a simple two-dimensional wavefunction propagation, could be used to study excited state dynamics in the butatriene cation;[77] this work expands dramatically on our previous report by demonstrating that the same GPR approach is suitable for performing MCTDH simulations, thereby opening up a wide range of future applications.

The remainder of this article is as follows. In the next section we will briefly recap grid-based dynamics methods, with particular emphasis on MCTDH. We then describe those aspects of GPR which are relevant to the construction of the PES or quantum dynamics, followed by details of the implementation of our MCTDH-based DD strategy. In Section 3, we present the results of dynamics calculations for the proton transfer in malonaldehyde and salicylaldimine, comparing the results of our new DD method with results obtained using pre-fitted PESs. We also demonstrate results of dynamics carried out on GPR PESs generated using *ab initio* electronic structure data generated "on-the-fly" (*i.e.* by direct interface to an electronic structure code during wavefunction propagation). Finally, we conclude by outlining work which will be carried out to further broaden the applicability of the method.

2 Methodology

2.1 Grid-Based Quantum Dynamics: The Standard Method and MCTDH

The theory of grid-based methods for solving the nuclear TDSE has been described in detail elsewhere;[7,78] here, we highlight those points most relevant to our proposed grid-based DD scheme.

Perhaps the most straightforward way to solve the nuclear TDSE is to expand a trial wavefunction in terms of a time-independent product basis, $\{\chi_{j_\kappa}^{(\kappa)}\}$,

$$\begin{aligned}\Psi(q_1,\cdots,q_f,t) &= \sum_{j_1}^{N_1}\cdots\sum_{j_f}^{N_f} C_{j_1,\cdots,j_f}(t)\prod_{\kappa=1}^{f}\chi_{j_\kappa}^{(\kappa)}(q_\kappa) \\ &= \sum_{J} C_J(t)\,X_J(\mathbf{q})\end{aligned} \tag{2}$$

where $\{C_{j_1,\cdots,j_f}\}$ is a set of complex, time-dependent coefficients and f is the number of DOFs in the system; we will discuss the nature of the basis functions later. We have also introduced the compound index, $J{=}j_1,\cdots,j_f$ on the second line of Eq. 2 to aid clarity in the expressions which follow. To model the dynamics we require equations-of-motion (EOMs) which can be integrated, and to obtain those we use the wavefunction *ansatz* of Eq. 2 in Dirac-Frenkel variational principle (DFVP),[79,80]

$$\langle\delta\Psi|\hat{H}-i\hbar\frac{\partial}{\partial t}|\Psi\rangle = 0. \tag{3}$$

After some algebra, we obtain the following EOM to describe the evolution of the wavefunction coefficients

$$i\hbar\dot{C}_J = \sum_L \langle X_J|\hat{H}|X_L\rangle C_L. \tag{4}$$

This set of coupled, first-order differential equations can be solved with standard integrators,

and with a sufficiently large basis provides a numerically exact solution to the TDSE. We will refer to this method for solving the TDSE as the standard method hereafter.

The standard method suffer from exponential scaling in computational effort as the number of DOFs is increased, meaning that for practical purposes f is limited to about 5. To reduce the effects of this scaling and expand the utility of quantum dynamics methods to larger molecular systems, the MCTDH method was introduced.[7] This method employs the following *ansatz* to represent the wavefunction

$$\begin{aligned}\Psi(Q_1,\cdots,Q_f,t) &= \sum_{j_1}^{n_1}\cdots\sum_{j_m}^{n_m} A_{j_1,\cdots,j_m}(t)\prod_{\kappa=1}^{m}\varphi_{j_\kappa}^{(\kappa)}(Q_\kappa,t)\\ &= \sum_{J} A_J(t)\,\Phi_J(\mathbf{Q},t)\,.\end{aligned} \tag{5}$$

Here, the wavefunction is defined as a linear combination of Hartree products of *time-dependent* basis functions; this is in contrast to the *time-independent* basis functions of Eq. 2. The basis functions, which are termed single-particle functions (SPFs), are functions of single modes of motion, each of which comprises a small number (typically from one to four) of individual DOFs (*i.e.* $Q_\kappa = (q_{\kappa_1},\cdots,q_{\kappa_p})$). Use of a time-dependent basis in MCTDH ensures that the number of basis functions can be kept small, meaning that the exponential scaling with system size which afflicts the standard method is minimized.

Individual SPFs are expanded in terms of an underlying, time-independent basis, $\{X_{i_\kappa}^{(\kappa)}\}$, the members of which are functions of the individual modes,

$$\varphi_{j_\kappa}^{(\kappa)}(Q_\kappa,t) = \sum_{i_\kappa}^{N_\kappa} c_{i_\kappa}^{(\kappa,j_\kappa)}(t)\,X_{i_\kappa}^{(\kappa)}(Q_\kappa)\,. \tag{6}$$

The basis functions used to represent the SPFs are the same as those used for expanding the wavefunction in the standard method (Eq. (2)). SPFs describing a mode which consists of more than one DOF are expanded in terms of products of basis functions along each DOF, much like the expansion of the total wavefunction in Eq. (2). The basis functions along each

DOF are standard, continuous functions, such as Hermite polynomials or sine functions, which are transformed into the so-called discrete variable representation (DVR), whereby the matrix elements of the position operator within the basis are generated and the resulting matrix diagonalised. The eigenfunctions, localised at evenly spread points in configuration space (hence forming a 'grid'), are the DVR basis functions. As these DVR functions are zero at all gridpoints except the one at which they are centred, the wavepacket is simply represented by the coefficients of each DVR basis function.

As with the standard method, a set of EOMs is needed to propagate the MCTDH wavefunction, and again the DFVP is used to derive these equations. This time we obtain two sets of EOMs, one for the wavefunction expansion coefficients, $\{A_J\}$, and another for the SPFs. In their most general form these equations read

$$i\hbar\dot{A}_J = \sum_L \langle\Phi_J|\hat{H}|\Phi_L\rangle A_L - \sum_{\kappa=1}^{f}\sum_{l=1}^{n_\kappa} g^{(\kappa)}_{j_\kappa l} A_{J^\kappa_l}, \tag{7a}$$

$$\begin{aligned} i\hbar\dot{\boldsymbol{\varphi}}^{(\kappa)} &= \left(1-P^{(\kappa)}\right)\left[\boldsymbol{\rho}^{(\kappa)-1}\langle\hat{H}\rangle^{(\kappa)} - \hat{g}^{(\kappa)}\mathbf{1}\right]\boldsymbol{\varphi}^{(\kappa)} \\ &\quad + \left(\hat{g}^{(\kappa)}\mathbf{1}\right)\boldsymbol{\varphi}^{(\kappa)}, \end{aligned} \tag{7b}$$

where $\hat{g}^{(\kappa)}$ is a constraint operator, present due to the redundancy in the *ansatz*, Eq. (5), from having both time-dependent coefficients and basis functions. In the EOM for the coefficients we also have $g^{(\kappa)}_{j_\kappa l} = \langle\varphi^{(\kappa)}_{j_\kappa}|\hat{g}^{(\kappa)}|\varphi^{(\kappa)}_l\rangle$ and $A_{J^\kappa_l} = A_{j_1,\cdots,j_{\kappa-1},l,j_{\kappa+1},\cdots,j_{n_\kappa}}$. In the EOM for the SPFs we use the projector onto the space of SPFs in mode κ, $\hat{P}^{(\kappa)}$, the inverse of the density matrix in that mode, $\boldsymbol{\rho}^{(\kappa)-1}$, and the mean-field matrix with elements, $\langle\hat{H}\rangle^{(\kappa)}_{jl}=\langle\Psi^{(\kappa)}_j|\hat{H}|\Psi^{(\kappa)}_l\rangle$. In this final expression we have used the single-hole functions $\Psi^{(\kappa)}_l = \sum_{J^\kappa} A_{J^\kappa_l}\Phi_{J^\kappa}$, where Φ_{J^κ} is the Hartree product of SPFs in all modes apart from mode κ.

Of crucial importance in the work we present here are the matrix elements involving the Hamiltonian operator in the EOMs above, in particular the potential energy term. To evaluate the matrix elements of the potential energy operator, $\hat{V}$, it is necessary to know the form of the PES, a function in all modes of the system, before carrying out the dynamics

calculations. The potential matrix elements are integrals over all DOFs (except mode κ in the case of the mean field operators in Eq. (7b)),

$$\langle \Phi_J | \hat{V} | \Phi_L \rangle = \int \cdots \int \Phi_J^* V\left(q_1, q_2, \cdots, q_f\right) \Phi_L \mathrm{d}q_1 \cdots \mathrm{d}q_f. \tag{8}$$

Evaluating this multidimensional integral is cumbersome and can become a bottleneck in the dynamics calculation. However, if we can represent the potential in the so-called sum-of-products form, where individual terms are just products of functions of the individual DOFs (not of the modes, which may contain more than one DOF), such as

$$V\left(q_1, q_2, \cdots, q_f\right) = \sum_i a_i \prod_{\kappa=1}^{f} V_i\left(q_\kappa\right) \tag{9}$$

where the coefficients, $\{a_i\}$, are independent of the DOFs, then the integral in Eq. (8) reduces to a sum-of-products of one-dimensional integrals

$$\langle \Phi_J | \hat{V} | \Phi_L \rangle = \sum_i a_i \prod_{\kappa=1}^{f} \int \varphi_j^{(\kappa)*} V_i\left(q_\kappa\right) \varphi_l^{(\kappa)} \mathrm{d}q_\kappa. \tag{10}$$

Evaluation of the matrix elements in this form is much less arduous than in the full-dimensional form, hence to fully exploit the efficiency of the MCTDH method it is best to represent the potential in the form given by Eq. (9). Incidentally, the same arguments about the form of the operator apply to the kinetic energy operator but, by choice of appropriate DOFs this will naturally be the case and hence the evaluation of kinetic energy matrix elements is usually straightforward.

The efficiency of evaluation of the PES integrals is increased still further, both for MCTDH and the standard method, by the use of DVR basis functions. In terms of the DVR grid-points the potential energy is diagonal such that, for two grid-points centred at $\mathbf{q}_\alpha$ and $\mathbf{q}_\beta$ we have

$$\langle \chi_\alpha | \hat{V} | \chi_\beta \rangle \approx V\left(\mathbf{q}_\alpha\right) \delta_{\alpha\beta}. \tag{11}$$

As such we only need to know the value of the PES at the coordinates of the grid-points to evaluate the PES matrix elements in the DVR basis.

2.2 Gaussian Process Regression

The key development reported here is the implementation of direct grid-based quantum dynamics using GPR.[64–71] This approach, in which *ab initio* electronic structure calculations at selected configurations are used to construct a global PES, provides a route to combining the power of grid-based quantum propagation with local electronic structure calculations; no prior fitting of the PES is required.

In our strategy, the PES is represented by a linear combination of Gaussian functions,[65] centred at a set of M reference points in configuration space, $\{\mathbf{q}^k\}$,

$$V(\mathbf{q}) \approx \sum_{k=1}^{M} w_k \exp\left(-\alpha|\mathbf{q}-\mathbf{q}^k|^2\right). \tag{12}$$

Here, the parameter α, which determines the width of the Gaussians, defines the length scale of the fit. If we use standard Cartesian or normal-mode coordinates, we can easily see that the expansion of the PES matches the sum-of-products form required for efficient MCTDH wavepacket propagation

$$V(\mathbf{q}) \approx \sum_{k=1}^{M} w_k \prod_{\kappa=1}^{f} \exp\left(-\alpha\left(q_\kappa - q_\kappa^k\right)^2\right). \tag{13}$$

The weights of the expansion in Eq. (12), $\{w_k\}$, are determined by solving the set of linear equations arising from requiring that the M PES values are reproduced at the M reference configurations, leading to

$$\mathbf{K}\mathbf{w} = \mathbf{b}, \tag{14}$$

where the elements of the vector, $\mathbf{b}$, are the values of the PES at M configurations, $\mathbf{q}^k$, for example calculated using an *ab initio* electronic structure program or from some fitted PES

function. Specifically, we have

$$b_i = V\left(\mathbf{q}^i\right). \tag{15}$$

The elements of the matrix, $\mathbf{K}$, multiplying the vector of GPR weights, $\mathbf{w}$, are a measure of the covariance between two members of the set of trial points,[65] given here as

$$K_{ij} = \exp\left(-\alpha|\mathbf{q}^i - \mathbf{q}^j|^2\right) + \gamma^2\delta_{ij}. \tag{16}$$

The parameter γ is typically chosen to be a small number and acts to regularise the matrix so that solution Eq. (14) is numerically well-behaved; more generally, γ can be viewed as representing the variance (or uncertainty) associated with the PES values in the vector $\mathbf{b}$ (thus, by choosing γ to be some small number in this work, we are implicitly assuming that the PES values are calculated to a high degree of accuracy, which is most often the case when using converged electronic structure calculations or an analytical PES).

In practice, GPR is straightforward to implement and, as noted above, is already in a form which is convenient for MCTDH simulations; however, the key outstanding issue is the choice of the M reference points used to construct the GPR PES. As noted previously, the wavefunction propagated in quantum dynamics simulations is non-local in nature, whereas *ab initio* electronic structure calculations provide the PES at specific local configurations. As a result, one approach to selecting the M reference points would be to simply choose the set of grid-points at which the time-dependent wavefunction would be expected to have non-zero value during the propagation; however, this approach is no better than the standard grid-based method and would be expected to suffer from a similar "curse of dimensionality".

Instead, a better strategy is to select the M GPR reference points in an adaptive manner during the wavefunction propagation, such that the PES is accurately represented where it is required for accurate propagation, namely in the vicinity of the time-dependent wavefunction; this then leads to the question of how one adaptively adds new configurations to the database of M GPR points during propagation. An obvious approach is simply to compare the

GPR PES and the calculated PES at grid-points encountered by the wavefunction during propagation, and then add the newly-calculated reference point to the database if the GPR PES is inaccurate beyond some threshold; however, as soon as one is required to calculate the (possibly computationally-expensive) underlying potential, then this point might as well be included in the database in any case.

In this work, we address this challenge by using the in-built error measure associated with GPR. In particular, exploiting the origins of GPR from the field of Bayesian statistics, it is straightforward to show that the GPR approach outlined above provides a direct way of assessing the accuracy of the approximate PES *without having to calculate the actual PES*. This is achieved using the following variance function which can be evaluated at any point in configuration space[65]

$$\sigma^2(\mathbf{q}) = 1 + \gamma^2 - \mathbf{k}^{\mathrm{T}}\mathbf{K}^{-1}\mathbf{k}. \tag{17}$$

The parameter, γ, is as defined in Eq. (16) as indeed is the matrix, $\mathbf{K}$. The elements of the vector, $\mathbf{k}$, are simply the covariances of the point of interest with the current set of M reference points; in other words, $k_i = \exp\left(-\alpha|\mathbf{q} - \mathbf{q}^i|^2\right)$. Thus, Eq. (17) provides a direct check of whether a new configuration, $\mathbf{q}$, should be added to the GPR reference points; if $\sigma^2(\mathbf{q})$ is greater than a threshold accuracy value, then the potential, $V(\mathbf{q})$, should be calculated and added to the GPR reference points. In this way, GPR provides an automated way of constructing a PES during wavefunction propagation; the implementation of this GPR PES construction approach in the context of standard and MCTDH quantum dynamics will now be discussed.

2.3 Implementation

Algorithms for carrying out DD, both for the standard method and MCTDH, with the PES calculated using GPR have been implemented in a development version of the *Quantics* package.[81] The quantum dynamics procedure, namely setting up the DVR basis, choice of

SPFs, initial wavefunction conditions and integration scheme (to integrate Eq. (4) or (7)), are as previously implemented in the package. We should note, however, that only the variable mean field integration (VMF) scheme has so far been implemented for solving the MCTDH EOMs with a GPR PES, with the constant mean field method[7] currently being modified.

Our current implementation of grid-based dynamics with "on-the-fly" GPR PESs, can use either atomic Cartesian coordinate or mass-frequency scaled normal modes as DOFs; this is currently for computationally simplicity, particularly because the kinetic energy operator for these coordinate choices are straightforward, but we emphasise that our approach can in principle be generalized to any appropriate coordinate system. In the case of normal mode coordinates, it is necessary to provide a transformation matrix between the scaled normal modes and the Cartesian coordinates, so that the Cartesian coordinates of the atoms can be passed to a relevant electronic structure program for the evaluation of the potential energy. The normal-mode transformation matrix can be generated by a standard normal-mode calculation at a chosen geometry-optimized reference configuration. On running a calculation, the chosen coordinate set defines the configuration subspace in which the GPR PES will be constructed; once this subspace has been defined by the user, along with the other parameters determining the nature of the (standard method or MCTDH) quantum propagation, the simulation can begin.

To initialise the GPR PES, assuming that we have no prior information about the PES, we adopt the following procedure. First, the effective width of the wavefunction along the i^{th} DOF is defined as

$$\langle \delta q_i \rangle = \left(\langle \Psi | \hat{q}_i^2 | \Psi \rangle - \langle \Psi | \hat{q}_i | \Psi \rangle^2 \right)^{1/2} . \tag{18}$$

Borrowing from the definition of normal distributions, we equate $\langle \delta q_i \rangle$ with the standard deviation, σ_i, of the wavefunction. For a normal distribution, 99.7% of the population is within $3\sigma_i$ of the mean, therefore we define the limits our sampling space for GPR PES generation along each DOF as $\langle q_i \rangle \pm 3\,\sigma_i$, *i.e.* the subspace within three standard deviations of the centre of the wavepacket. An initial PES evaluation is performed at the molecular

geometry corresponding to the "centre" of the wavepacket, $\langle \mathbf{q} \rangle$. Subsequently, N additional configurations are generated by random uniform sampling for each DOF within the limits of the sampling subspace defined by the wavepacket centre and standard deviations; in all calculations reported here, we use $N = 100$, such that the initial set of reference points in the GPR PES is $M = 101$. The potential is then calculated at each reference geometry, for example using an analytical PES or *ab initio* electronic structure calculations, hence giving the vector, $\mathbf{b}$, of potential values at the reference points (Eq. (15)). The M reference points in configuration space are then used to evaluate the matrix $\mathbf{K}$ defined in Eq. (16) (using, in this work, a length parameter $\alpha = 0.5$) and the linear equations of Eq. (14) are solved to give the initial vector of GPR weights, $\mathbf{w}$. The solution of the GPR equation is carried out using Cholesky decomposition routines implemented in LAPACK.[82] Once the initial weights have been determined, we then have an initial expression for the GPR PES using Eq. (12).

Following the formation of the initial GPR PES, the wavefunction time-propagation is allowed to proceed. For each of the M potential terms, there are f individual components in the Gaussian functions Eq. (13)), one for each DOF in the system. If a mode in the MCTDH wavefunction, Eq. (5), comprises a single DOF (*i.e.* the SPFs in that mode are one-dimensional functions) or a standard method calculation in one-dimension is being performed, then the value of the individual potential term is simply evaluated at each of the grid-points defined by the DVR basis in which the SPFs or wavefunction are expanded (Eq. (6)) following Eq. (11). If a multi-dimensional standard method wavefunction or an MCTDH mode comprising more than one DOF (*i.e.* the SPFs are multi-dimensional functions) is being considered then the grid-points in Eq. (2) or Eq. (6) are defined by the corresponding number of coordinates. The GPR PES at these grid-points is then evaluated using Eq. (13). Having completed the procedure of evaluating the potential matrix elements in the DVR basis, the dynamics proceeds in the usual way; in the MCTDH case, these matrix elements are transformed to the SPF basis before being used to generate the EOMs (Eq. (7)), which are then integrated. In the standard method, the matrix elements are used directly in Eq.

(4).

The propagation could be allowed to proceed using just the initial set of points to define the GPR PES but, as the wavepacket evolves, the representation of the PES given by sampling configuration space with reference to the initial wavepacket is likely to become increasingly inaccurate; obviously, it is necessary to generate a new representation of the PES which better reflects the regions of configuration space being sampled during the dynamics. It is, of course, possible to generate a new set of random configurations at some sensible time-interval in the propagation time and to calculate N new PES values, discarding the previously obtained information about the PES. However, we take a different approach which is based on the "grow" methodology of Collins and coworkers,[83,84] and is similar to that used in the DD-vMCG method implemented in the *Quantics* package.

In the approach adopted here, the initial potential values are stored in a database along with the molecular geometries at which they were calculated (the information is held in memory during the propagation but also output to file for re-use in subsequent calculations if needed). The database of configurations and potential energy values is augmented at regular intervals during the wavepacket propagation by the sampling of configuration space around the centre of the wavepacket in the same way as the initial sampling. At each of the sampled configurations, the GPR variance as defined in Eq. (17) is calculated (using the database points from previous evaluations only, so as to avoid repeated matrix inversions). If the variance is below some threshold (in this work taken to be 10^{-6}), then it is considered that the current GPR PES representation at that configurations is sufficiently accurate, such that no new potential energy values need to be calculated. However, if the variance is greater than the threshold, then a new energy is calculated and stored in the database. Once any new points have been added to the database, Eq. (14) is solved once again (including all energies in the database) to give a new set of GPR weights and hence a new form for the PES. The wavepacket propagation then proceeds, adding new database points and updating the PES as necessary until completion. In this way, we combine grid-based wavefunction

propagation with "on the fly" evaluation of the PES; furthermore, as noted above, the GPR PES constructed using the potential energy evaluations is already in a form which is convenient for MCTDH propagation.

Naturally, the PES available during the early stages of the propagation is likely to be less accurate than that constructed later in time, when more database points are used to generate the GPR PES; as a result, once an initial calculation is complete, it is possible to re-run the dynamics using the *full* database from the start. This second propagation can be run without adding any new points to the database or with the option of adding new database points according to the threshold conditions outlined above. In principle the propagation could be repeated in the latter manner until no more points are added and the GPR PES can be considered converged (at least for the regions of configuration space sampled during the total propagation time with the same initial wavepacket conditions). In the simulations reported below, single calculations have been performed to generate the PES before subsequent wavepacket propagations using the database created during the prior calculation.

Finally, to calculate potential energy values at sampled configurations during wavefunction propagation, our implementation uses much of the machinery in *Quantics* put in place to perform DD-vMCG calculations by interfacing with assorted *ab initio* electronic structure programs. In practice the program creates an input file at the geometry of interest, calls the external quantum chemistry package, then reads the appropriate information (in the case considered here, just the total electronic energy) from the resulting output file. Furthermore, we note that we can also perform GPR PES-based simulations of *any* PES, not just those generated by electronic structure calculations; this fact is used later to benchmark our new simulation strategy for PESs which were previously fit to analytical functions.

3 Results

To demonstrate the abilities of our direct grid-based dynamics methods, the ground-state dynamics of the intramolecular proton transfer for two different molecules has been studied. Such processes are characterised by the double-well nature of the PESs on which they occur, arising from two local minima corresponding to the hydrogen bonded to different atoms, separated by a potential barrier. Double well potentials are ideally suited to testing new quantum dynamics methods because they often feature strongly quantum-mechanical tunnelling processes which are difficult, if not impossible, to accurately reproduce *via* other non-quantum methods.

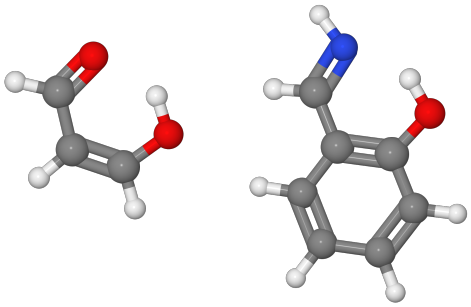

(a) (b)

Figure 1: Two molecules of interest in this work: (a) Malonaldehyde and (b) Salicylaldimine. In both case the dynamics of the transfer of the proton bonded to an oxygen atom in these pictures is considered; in the former case to the other oxygen and in the latter to the nitrogen.

3.1 Malonaldehyde

As the first test of our grid-based DD method, we consider the ground electronic state dynamics of the intramolecular proton transfer in malonaldehyde (Fig. 1(a)). The aim of this study is to test the ability of dynamics performed on a GPR approximation to the PES to replicate those observed on a known PES. In this way, we can directly assess whether surfaces generated using our GPR method are accurate representations of the underlying PES.

Recently, an accurate PES for the ground state of malonaldehyde was reported by Mizukami *et al*, fitted to energies calculated at the HF/QZVPP level with fc-CCSD(T)(F12*)/def2-TZVPP correlation energies.[72] We have integrated the subroutine published by them into the *Quantics* package so as to be able to generate potential energies at molecular geometry sampled by the dynamics, and hence be able to run dynamics using either the fitted PES or the direct dynamics approach using a GPR PES.

Two calculations were performed on a 3-dimensional subsystem of malonaldehyde, both using the standard method (Eq. (2)), the first just using the full Mizukami PES (evaluated on all grid-points) and the second using a GPR representation of the PES generated "on-the-fly" using the implementation described in Section 2.3. The dynamics was performed in dimensionless, mass-frequency scaled normal mode coordinates, where the normal mode transformation matrix was calculated by diagonalising the mass-weighted Hessian matrix determined at the proton transfer transition state geometry given previously.[72]

The three normal modes chosen to carry out the dynamics were the proton transfer mode (v_1 of frequency $1321.32i\,\mathrm{cm}^{-1}$), the out-of-plane motion of the proton (v_{12} of frequency $1290.31\,\mathrm{cm}^{-1}$) and the in-plane OHO bending mode (v_{18} of frequency $1899.62\,\mathrm{cm}^{-1}$). For both calculations a sine DVR basis with 101 grid-points was used for v_1 and a harmonic oscillator DVR basis was used for the other modes, with 21 functions each. The initial wavepacket was constructed as a Gaussian function of width 0.7 along all modes, centred at v_1=0.5 and v_{11}=v_{18}=0.0. The dynamics was run using the short iterative Lanczos propagator of order 15, and was followed for 100 fs. In the case of the direct dynamics calculation, the PES was sampled, as described in Section 2.3, every 1 fs.

First, we compare the vibrational spectrum of the 3-dimensional malonaldehyde model calculated using the full grid-based standard method and our GPR-based DD method. This spectrum was calculated by Fourier transforming the autocorrelation function, defined as

$$G\left(t\right) = \langle \Psi(0) | \Psi(t) \rangle. \tag{19}$$

The value of $G(t)$ was output every 1 fs during the course of both calculations. The procedure for performing this transform is described in detail elsewhere, particularly concerning the use of a damping function to ensure that the function reaches zero at the end of the propagation in order to avoid artefacts in the spectrum.[7]

In Fig. 2, we present the vibrational spectra of 3-mode malonaldehyde resulting from these two calculations. Clearly, the two spectra are in excellent agreement, with each showing four main peaks. The most intense peak in both cases is centred at 2949 cm^{-1}, the intensity of the peak differing by less than 3% between the two calculations. The next two peaks in increasing energy order do not quite coincide between the calculations, the GPR peaks being centred 6 cm^{-1} lower in energy than those from the full calculation in both cases, but again have very similar intensities. The highest energy peak around 5040 cm^{-1} differ in position by 13 cm^{-1} between the calculations and by 12% in intensity.

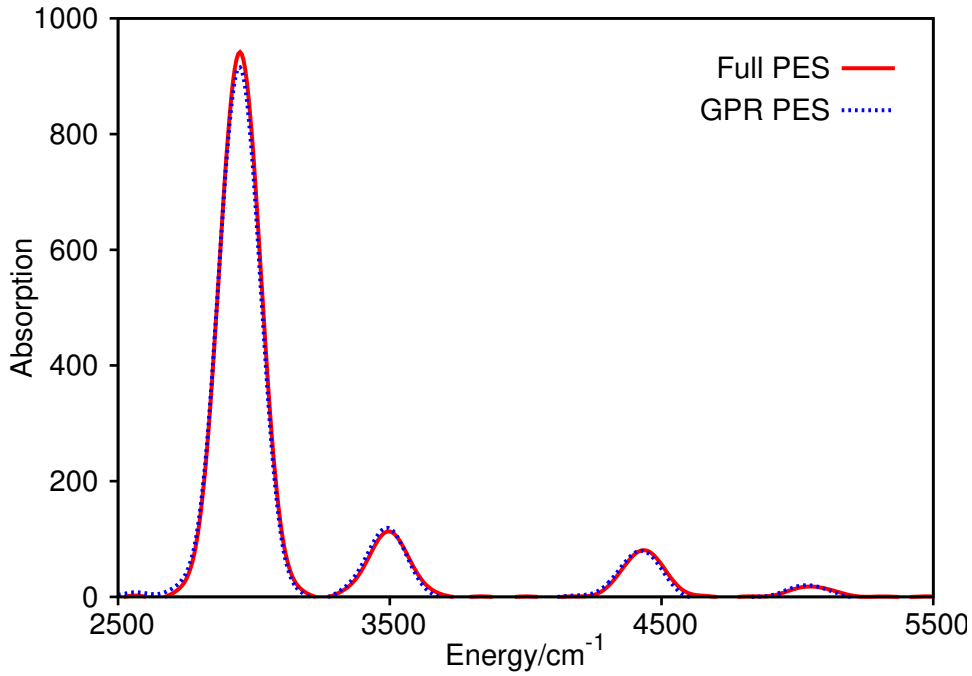

Figure 2: Vibrational spectra of a three-mode model of malonaldehyde. All potential energies were calculated from the surface of Mizukami *et al.*[72] The solid, red line is the result of the calculation performed using the full dynamics. The dashed, blue line is the result of the calculation with the potential constructed using the GPR process, sampling points in configuration space as explained in the text. The energy origin is the transition state energy.

Overall, the differences between the spectra are very small, indicating that the GPR representation of the PES is very accurate. The discrepancies, in the energies and intensities of the peaks, between the two calculations are simply due to the small variation in the shape of the PES, leading to small shifts in the vibrational energy levels. This is particularly so early on in the wavepacket propagation, where fewer energy points have been calculated and hence the number of terms in Eq. (12) is less.

We have implied that the representation of the GPR PES at later stages in the propagation should be more accurate than that at earlier times due to the addition of extra reference configurations to the GPR expansion; this point is clearly demonstrated in the next comparison. During the initial DD calculation, 2425 points in configuration space were sampled; as noted in Section 2.3, the calculated potential energies are saved on file and can be re-used in subsequent calculations. To this end, a second propagation was run, using a GPR PES calculated at the start of the propagation using all 2425 reference energies; no further points were added during this second propagation. The resulting spectrum is visually identical in shape to that resulting from the full calculation, all peaks aligning with one another exactly. The intensities of the lowest energy peak differ between the two calculations by only 0.015% whilst those of the highest energy peak differ by less than 3%. This result indicates that, given an adequate sampling of configuration space, GPR can reproduce the shape of the underlying PES almost exactly.

A more sensitive test of the dynamics than the vibrational spectrum is the measurement of the wavepacket flux through a dividing surface. The flux can be measured as the rate of change of wavefunction population in the region beyond the dividing surface.[7] Using a step function defined along some DOF, $\theta\left(q-q_{\gamma}\right)$, where q_{γ} is the coordinate of the dividing surface, the population to the positive side of the surface is $\langle\Psi|\theta\left(q-q_{\gamma}\right)|\Psi\rangle$. Applying Ehrenfest's theorem,[78] the rate of change of the population is[7]

$$\frac{\mathrm{d}}{\mathrm{d}t}\langle\Psi|\theta\left(q-q_{\gamma}\right)|\Psi\rangle=\frac{i}{\hbar}\langle\Psi|[\hat{H},\theta\left(q-q_{\gamma}\right)]|\Psi\rangle \tag{20}$$

The flux operator is thus defined as $\hat{F}=\frac{i}{\hbar}[\hat{H},\theta\,(q-q_\gamma)]$.

The flux expectation value was evaluated every 1 fs during the three wavepacket propagations described above, with the dividing surface placed perpendicular to the v_1 mode at the location of the transition state between the two equivalent isomers (*i.e.* v_1=0). Figure 3 shows the calculated flux expectation values for the three calculations: standard method dynamics on the full PES, single-run GPR-based DD propagation, and GPR-based DD propagation using previously-sampled energies. Comparing these results, it is clear that DD accurately reproduces the quantum dynamics of the system as the wavefunction propagates. In all three cases, there is an initial movement of the wavepacket from the right-hand side of the barrier (positive v_1 coordinate) towards the left-hand potential well, followed by a periodic crossing and re-crossing with period of just over 40 fs. This process involves tunnelling through the barrier, demonstrating that our DD method can cope with this feature of dynamics; in other words, the GPR PES describes the two potential wells and the potential barrier with sufficient accuracy to reproduce the correct wavefunction tunnelling.

As with the vibrational spectrum, there is very good agreement between the results of the full dynamics and those of the *initial* DD run. Not only is the overall form of the time-dependent flux reproduced, but small features such as the spikes in flux during the first 10 fs are also reproduced. The flux calculated using DD on the final database gives even better agreement with the results from the full dynamics. The agreement is not perfect, with some small discrepancies creeping in particularly at later times (for example the small plateaus in the flux at about 45 fs and 50 fs are not seen in either DD calculation, and some of the fine structure towards the end of the propagation is missing). However, the ability of the DD method to reproduce the wavepacket flux accurately is a further indication that the GPR PES is a faithful representation of the PES being sampled.

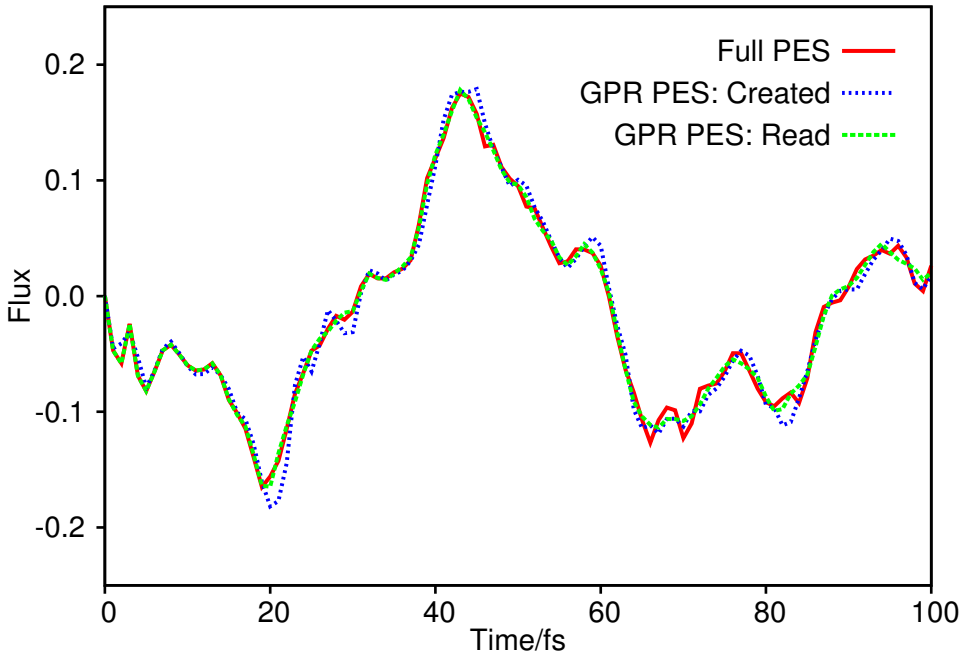

Figure 3: Plot of the flux operator expectation value, $G(t)$, for a three mode model of malonaldehyde. The dividing surface is placed at the barrier of the transition mode, v_1. All potential energies were calculated from the surface of Mizukami *et al.*[72] The solid, red line is the result of the calculation performed using the full dynamics. The hashed, blue line is the result of the calculation with the potential constructed using the GPR process, sampling points in configuration space as explained in the text. The dashed, green line is the result of the calculation with the potential constructed using GPR process on a pre-calculated database of potential energies.

3.2 Salicylaldimine

As a second test system, we look at the proton transfer process in salicylaldimine (Fig. 1(b)). Here, the proton moves between the oxygen atom (the imine or enol form) and the nitrogen atom (the amine or keto form), the former being the more stable structure of the two. In contrast to malonaldehyde, there are thus two distinct tautomers to consider, and the PES is not symmetric about the barrier separating the energy minima which correspond to each tautomer.

An analytical PES, fitted using the VCHAM approach for 13 of the normal modes of salicylaldimine (calculated at the transition state geometry between the optimised keto and enol forms), was recently published by Polyak *et al*[60] and it is this PES that we use to

compare the standard, grid-based dynamics and DD results. Contrary to the original report, the 3-21G basis set was used along with the restricted Hartree-Fock method to generate energies to which the PES was fitted. In this work we will use the previously-fitted PES to generate benchmark results against which to compare our DD scheme. We consider two cases here: (i) a two-dimensional version, which is sufficiently small that the standard (grid) method of propagation can be used (thereby minimizing errors arising due to wavefunction propagation itself, allowing us to focus on the accuracy with which GPR can reproduce the underlying PES), and (ii) a six-dimensional version, where we use MCTDH, combined with GPR, to perform quantum dynamics "on the fly". Furthermore, we will also compare these results to GPR PESs calculated by direct interface with an external *ab initio* electronic structure code, in this case ORCA,[85] marking the first time that MCTDH simulations have been performed "on the fly".

3.2.1 2D Dynamics

The first comparison we make uses a two-dimensional model of salicylaldimine, the normal modes chosen being those termed v_1 and v_{36} by Polyak *et al*; these are the proton transfer mode and in-plane OHN bending mode, respectively. As only two DOFs were involved in the calculation, it was possible to run standard method dynamics for (i) the full fitted PES, (ii) a GPR PES representation generated in DD simulations of the fitted Polyak surface, and (iii) a GPR PES representation generated using DD simulations and electronic structure energies calculated "on-the-fly". All calculations used a sine DVR basis with 121 functions along the v_1 mode and a harmonic oscillator DVR basis comprising 21 grid-points along v_{36}. The initial wavepacket was constructed as a 2D Gaussian function centred at v_1=0.96 and v_{36}=0.14 with widths $\langle \mathrm{d}v_1 \rangle$=0.5706 and $\langle \mathrm{d}v_{36} \rangle$=0.7704. This starting configuration places the system to the enol side of the barrier between the two tautomers (the transition structure is at the origin of the coordinate system). Propagations were performed for 100 fs with data output every 1 fs, using the default integrator options in *Quantics* (see Section 3.1).

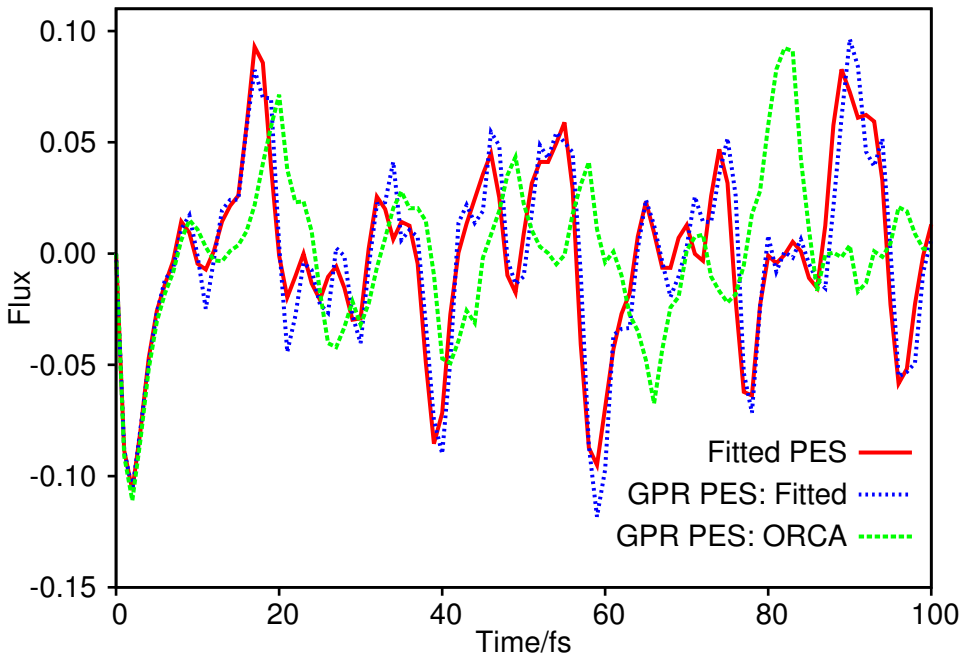

Figure 4: Plot of the flux operator expectation value for a two degree-of-freedom model of salicylaldimine. The dividing surface is placed at the barrier of the transition mode, v_1. The solid, red line is the result of using the full dynamics. The hashed, blue line is the result of the calculation with the potential constructed using the GPR process, sampling points in configuration space as explained in the text. In both cases the potential energies were calculated from the surface of Polyak *et al.*[60] The dashed, green line is the result of the calculation with the potential constructed using the GPR process, with energies calculated by calls to ORCA, "on-the-fly".

Figure 4 shows the wavefunction flux through a surface perpendicular to the proton transfer mode, placed at the peak of the transition barrier between the tautomers (v_1=0), allowing us to follow the tautomerization process over the course of the propagation time; results are shown for all three calculations. We first compare the flux of the wavefunction moving on the fitted surface to the wavefunction flux on the PES approximated using GPR sampling on the fitted PES. Clearly the two curves are very similar to one another; the initial, negative flux indicating proton transfer across the potential barrier towards the keto tautomer, followed by a re-crossing of the barrier to the enol side. Later in the dynamics there are short periods of crossing one way or the other, each lasting only a few femtoseconds. However, the most important point to note is that the two calculated fluxes follow each other

very closely for the entire duration of the dynamics. The correspondence is particularly good early in the dynamics, degrading slightly at later times, with the flux on the GPR PES lagging behind that on the full, fitted PES. In the DD GPR simulation, 353 potential energies were calculated during the course of the propagation; as expected, restarting the simulation using this full GPR reference set (not shown) gives even better agreement with that calculated using the full fitted surface. The results from the initial comparison reinforce the conclusion drawn from the calculations on malonaldehyde, namely that a GPR PES can give a very good representation of the underlying PES. As an aside, we note that our GPR PES scheme required far fewer PES evaluations than the total number of grid-points in this two-dimensional case ($21 \times 121 = 2541$).

The second comparison we can make when examining Fig. 4 is between the fluxes calculated using the fitted PES and the flux determined from dynamics performed on a GPR PES calculated using *ab initio* energies evaluated "on-the-fly". In constructing the *ab initio* GPR PES, the sampling of configuration space around the wavepacket centre is performed in the same way as described in Section 2.3; however, the potentials are calculated using RHF/3-21G so as to match the level of theory used by Polyak *et al* in performing their DD-vMCG calculations. From Fig. 4, during the first 10 fs or so, the flux follows that calculated using the fitted potential (*i.e.* the initial crossing to the keto side of the barrier); however, after this point the flux diverges from that calculated using the fitted surfaces. This plot can be best compared to Fig. 4(d) in the Polyak paper,[60] where a DD-vMCG calculation was performed for this system; specifically, the difference between the *ab initio* and fitted PES observed in our DD simulations are similar to the differences observed between the DD-vMCG result using "on-the-fly" PES evaluation and vMCG using the fitted PES. In this previous work, the discrepancy between the two results is attributed to the form of the potential on the enol side of the barrier which made the fitting of the potential along the υ_{36} difficult for the VCHAM method. The flux calculated using a potential constructed by an interpolation type method, as is done using GPR or the Shepard interpolation used when

performing DD-vMCG calculations, should thus be a more accurate reflection of the true dynamics. This result, and the comparison to previous DD-vMCG results, clearly shows that it is possible to perform direct grid-based dynamics calculations using a PES generated "on-the-fly" using *ab initio* data.

3.2.2 6D Dynamics

The second set of calculations performed on salicylaldimine uses six normal modes; two of these are the same as in the 2D case above (ν_1 and ν_{36}), with the four additional modes labelled ν_{10}, ν_{11}, ν_{13} and ν_{32} in the work by Polyak *et al* (see Fig. 2 in reference 60 for diagrams of the motions, all of which are in-plane modes). We note that these six modes are the same as those considered in previous DD-vMCG simulations. We perform the same comparison as performed in the previous section; specifically, we compare (i) dynamics on the fitted PES, (ii) dynamics on a GPR approximation to the fitted surface, and (iii) direct-dynamics with a GPR approximation to the PES generated by "on-the-fly" electronic structure calculations. In the 6D case, however, there are too many DOFs to use the standard grid-based wavefunction propagation method, so we use MCTDH for all three calculations.

Following previous simulations of salicylaldimine, our calculations all used a wavefunction *ansatz* constructed in terms of three sets of 2D SPFs, with the DOFs being grouped as $\{\nu_1, \nu_{36}\}$, $\{\nu_{10}, \nu_{11}\}$ and $\{\nu_{13}, \nu_{32}\}$. The propagations were run for 100 fs using the Adams-Bashforth-Moulton predictor-corrector integrator of sixth order to solve the EOMs using an accuracy parameter of 10^{-5} (these settings are the default for the VMF integration scheme in *Quantics*). The MCTDH calculation on the fitted PES used 18 SPFs in each mode, and the calculations using the GPR approximation to the PES (both to the fitted PES and to the *ab initio* points) required 30 SPFs per mode. This increase in the number of SPFs was necessary due to the highly correlated nature of the form of the potential when using GPR (*i.e.* all DOFs are coupled, being involved as they are in all potential terms, whereas the fitted PES couples at most two DOFs per term). The basis of grid-points used to expand

the SPFs was a set of 101 sine DVR functions along ν_1 and 21 harmonic oscillator DVR functions along the other five modes. The initial wavepacket was centred at $\langle\nu_1\rangle$=0.96, $\langle\nu_{36}\rangle$=0.14, and $\langle\nu_{10}\rangle$=$\langle\nu_{11}\rangle$=$\langle\nu_{13}\rangle$=$\langle\nu_{32}\rangle$=0.0, with widths of $\langle\delta\nu_1\rangle$=0.5706, $\langle\delta\nu_{10}\rangle$=0.7745, $\langle\delta\nu_{11}\rangle$=0.7590, $\langle\delta\nu_{13}\rangle$=0.6902, $\langle\delta\nu_{32}\rangle$=0.6707 and $\langle\delta\nu_{36}\rangle$=0.7704.

In Fig. 5 we present two plots showing results from these calculations; both show plots of the wavepacket flux through a dividing surface perpendicular to the stretching mode, ν_1, and at the peak of the transition barrier (as in the 2D case). Looking first at Fig. 5(a) we show the results of: (i) the MCTDH calculation on the fitted PES (the full result), (ii) the initial MCTDH calculation using a GPR approximation to the fitted PES (with electronic energies being added every 1 fs), and (iii) an MCTDH calculation performed using the GPR approximation to the fitted PES, using the database created by the previous calculation. In Fig. 5(b) we repeat the plot of the full result for clarity along with a plot of the flux generated by an MCTDH calculation using a GPR PES generated by calculating RHF/3-21G electronic energies with ORCA "on-the-fly" (the database is updated every 1 fs). Again, Fig. 5(b) also shows the flux for a subsequent calculation employing MCTDH using a GPR PES constructed using the database of energies created in the previous calculation.

Making an initial comparison of the plots in Fig. 5 with those in Fig. 4, we see that, after an initial move towards the keto isomer (indicated by the negative flux), there is far less overall movement of the wavepacket across the potential barrier in the 6D case than in the 2D case across the 100 fs period of simulated dynamics. The reason for this is that the presence of more DOFs, each of which is coupled to the others, allows the wavepacket to spread and move in directions which do not take it over the barrier; in the 2D case the wavepacket is constrained to move in only two directions, one of which is across the barrier where the flux is being measured, so more structure is seen in Fig. 4 than in Fig. 5.

Looking now at each figure in turn, we begin with Fig. 5(a) where the dynamics in all three calculations was based on the fitted PES of Polyak *et al.*[60] The solid, red line is the full MCTDH result, the benchmark against which the other two plots in the figure should

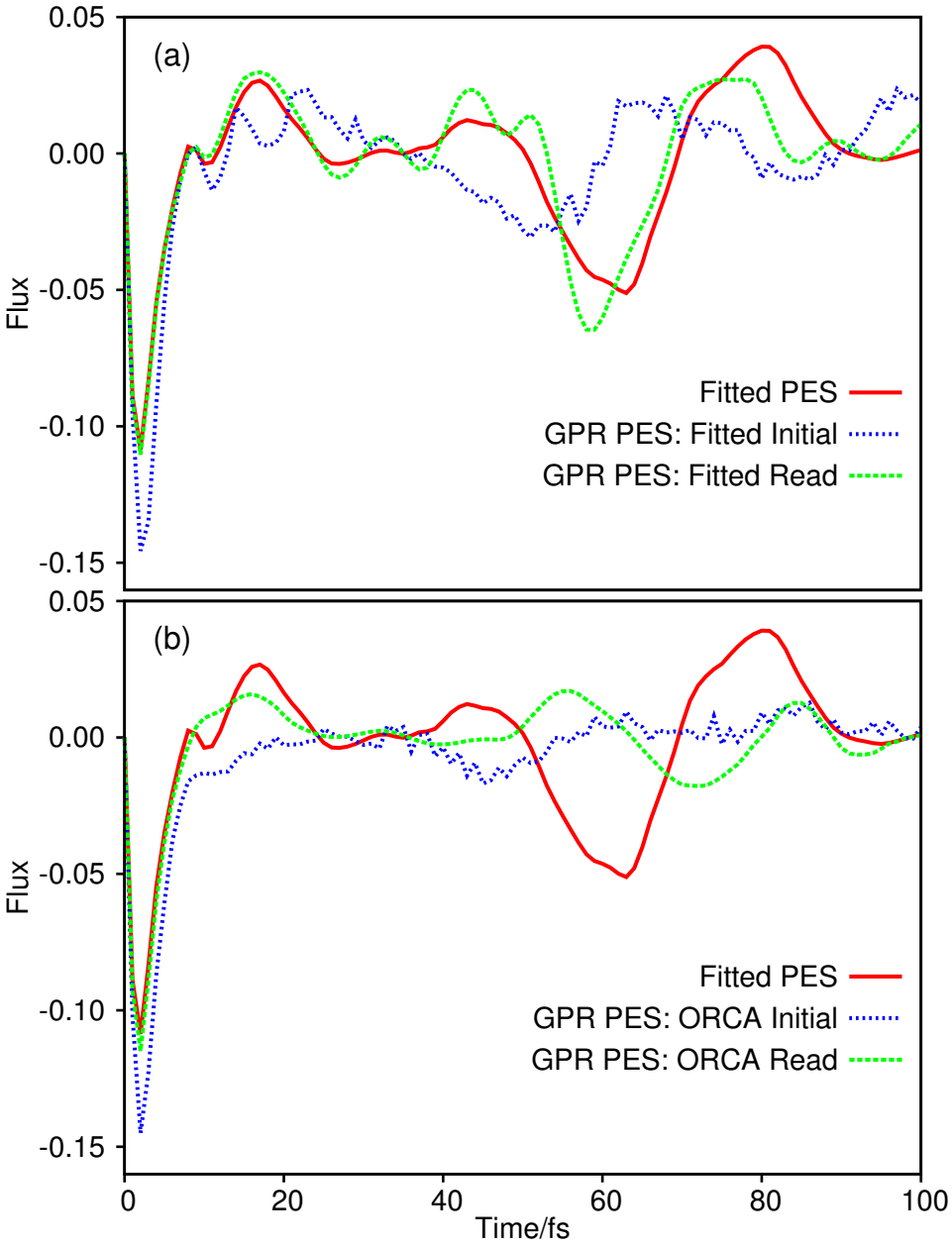

Figure 5: Plots of the flux operator expectation value for a six degree-of-freedom model of salicylaldimine. The dividing surface is placed at the barrier of the transition mode, ν_1. The solid, red line in both plots is the result of using the full dynamics. In plot (a) the hashed, blue line is the result of the calculation with the potential constructed using the GPR process with energies being calculated from the fitted PES of Polyak *et al.*[60] The dashed, green line is the result of a subsequent calculation using a GPR representation of the PES generated by the database of points calculated during the initial calculation. In plot (b) the hashed, blue line is the result of the calculation with the potential constructed using the GPR process, with energies calculated by calls to ORCA, "on-the-fly"; the dashed, green line shows results given by a calculation run on the PES generated by the previous calculation with no further database points added.

be compared. The full MCTDH result indicates an initial, rapid flow of the wavepacket over the barrier towards the keto tautomer, followed by an oscillation back towards the enol form; all of this occurs within the first 10 fs of the dynamics. There is a subsequent, small move in the same direction followed by motion in the positive flux direction towards the enol tautomer around 20 fs. This motion slows to close to zero until there is more motion in the enol direction between 40 and 50 fs, followed by a 20 fs period of movement in the keto direction (the trough centred on 60 fs). The most significant move towards the enol side of the potential barrier of the whole dynamics occurs around 80 fs. The final 10 fs of the dynamics is characterised by a lack of motion across the barrier.

Examining the results of the initial calculation using a GPR potential (hashed, blue line in Fig. 5(a)), where potential energy values from the fitted PES were added every 1 fs during the dynamics, we see that the initial motion of the wavepacket across the barrier to the keto tautomer is qualitatively correct, if somewhat overestimated. The plot rejoins that of the full result around the 10 fs point, and there is a subsequent, small motion towards the keto tautomer, again, as seen in the full result but likewise overestimated. As with the full result, the flux then heads in the positive direction, but unlike the full result, it quickly falls back to zero. From this point on, the two plots do not closely correspond; the flux of the GPR calculation turns negative between 30 and 60 fs before going positive until 80 fs, then back to zero and finally into the positive region to the end of the calculation. Clearly the *initial* potential generated "on-the-fly" is not accurate enough to closely reproduce the flux of the full result but, at the same time, not so inaccurate as to get the dynamics completely wrong.

To further assess the accuracy of the GPR PES, the dynamics was repeated using a GPR PES calculated using the energies generated during the initial propagation; the results of this are shown by the dashed, green line in Fig. 5(a). It is immediately apparent that the dynamics much more closely matches the full result than the initial calculation. The first 10 fs of the plot almost exactly matches the that of the full result, whilst the period of positive flux between 10 and 20 fs is accurately replicated. From that point onwards the flux

qualitatively matches that of the full result, in particular the period of negative flux between 50 and 70 fs and that of positive flux for the 20 fs afterwards correspond to the full result quite well. The match is not perfect, but it is clear that the underlying dynamics is well represented; in other words, the GPR procedure gives a good approximation to the potential from which it is derived.

In spite of this success, these MCTDH results highlight one downside of our method, namely the growth in the number of Gaussians needed to represent the PES. Recall from Section 3.2.1 that 353 Gaussians were needed to accurately represent a 2D PES, whilst in section 3.1, 2425 Gaussians were needed for a 3D PES (admittedly for a different molecule). In this 6D calculation, 10101 database points were generated, the maximum possible in this particular calculation (an initial point at the wavefunction centre, then 100 points at each femtosecond, 0 to 100). Clearly the number of Gaussians needed to accurately represent the PES increases rapidly as the dimensionality of the problem rises. This is less of an issue when using the standard method for the dynamics as it is only necessary to know the actual value of the potential at the location of each DVR point, not the contributions from each Gaussian in the GPR; the PES in that case is completely determined by a single number for each gridpoint, which can be evaluated and saved whenever the energy database is updated. On the other hand, the structure of the MCTDH EOMs means that it is the value of each term in the GPR expansion of the potential along the DOFs making up each set of SPFs that is required; in other words the potential has to be dealt with term by term. In the case of 6D salicylaldimine, there are thus 10101 terms in the potential which have to be calculated and then combined in the Hamiltonian and mean-field integrals in Eq. (7). This number of terms in the potential operator means that calculations become very time-consuming as more DOFs are added; we come back to this point later.

Moving on to consider Fig. 5(b), we note the same issues with computational effort, as just outlined, when propagations are performed using a GPR PES generated using *ab initio* energies calculated "on-the-fly" using ORCA. Again, 10101 database energies were

calculated, each of which naturally required a call to the ORCA program. As with Fig. 5(a) the solid, red line is the result of the flux for the MCTDH calculation on a *fitted PES*, repeated for clarity in comparison with the new results performed on an *ab initio* GPR PES. The first new result to examine is that represented by the hashed, blue line, which is generated by performing dynamics on a GPR PES built from *ab initio* energies added to an initially empty database. As with the calculations using the fitted surface (Fig. 5(a)), we see an overestimated negative flux during the first 10 fs, which does not quite return to zero at 10 fs, but slows down there, only reaching zero after about 25 fs. From this point onwards the flux is fairly featureless, staying close to zero, except for a short period of negative flux between 40 and 50 fs. The plot is not particularly smooth (as in the corresponding plot in Fig. 5(a)) because the updates to the potential at every femtosecond cause the global PES to shift slightly, hence affecting the motion of the wavepacket.

The dashed, green line represents the results of the subsequent calculation using a GPR PES based on the 10101 *ab initio* energies calculated during the previous propagation. Here the initial period of negative flux matches that of the MCTDH calculation on the fitted surfaces, both in intensity and duration. The flux is then positive until 25 fs and then returns to zero until about 50 fs. The flux then has a bump upwards into positive territory until about 60 fs, before a period in the negative direction for the next 20 fs, then a final up and down to the end of the propagation. Clearly the dynamics does not match that of the full (MCTDH, fitted surface) result, but it should not be expected to because the GPR PES in this case is an interpolation of the actual HF/3-21G PES, rather than of a fitted approximation to it. The close agreement in the first few femtoseconds occurs when the wavepacket is localised relatively close to the origin of the coordinate system, the point around which the VCHAM fitted potential is expanded. The fit will be most accurate around this region, *i.e.* most closely resembling the interpolation of the GPR, hence the similarity in the dynamics. The differences in the potential are more pronounced further from this point, in regions where the wavepacket explores later in the propagation. The plots in Fig. 5(b)

are best compared to Fig. 6 in Ref. 60, where a DD-vMCG calculation on the same system was performed. Making this comparison, we see that the plots of the flux match really quite well with the DD-vMCG results, with the major features reproduced. This indicates that the approach outlined here, using electronic energies calculated "on-the-fly", gives dynamics which closely agree with those from a well established alternative DD method.

As a final note, it is worth commenting on the computational effort of these simulations. The 6D MCTDH simulation coupled to HF/3-21G calculations took approximately 186h walltime on the first run and then 639h for the run using the pre-calculated database; both were parallelised across 16 processors. The 6D MCTDH calculation on the original fitted PES required 69h walltime for the run generating the database of points with the second calculation taking 143h (again both were parallelised over 16 processors). However, the important point of our approach is that the PES is generated "on the fly"; there is no need for laborious pre-fitting of the PES, and the associated challenges surrounding appropriate choice of coordinates, functional forms, and so on. As a result, and bearing in mind that the approach highlighted in this Article is far from optimized with regards to both methodology and code implementation, we expect that our DD MCTDH scheme to quickly evolve into a useful and highly-accurate computational tool for studying quantum dynamics in both ground-state and excited-state systems.

4 Conclusions

We have presented initial results for a new direct quantum dynamics scheme which combines well-established grid-based dynamics methods (standard method and MCTDH) with PESs created using GPR with electronic energies calculated "on-the-fly" either from a pre-fitted potential or from an electronic structure package. To the best of our knowledge, this is the first implementation of a DD version of MCTDH.

In calculations on a 3D model of malonaldehyde and a 2D model of salicylaldimine, we

have shown that the GPR representation of the PES is capable of almost exactly matching the underlying potential by comparison to results from pre-fitted PESs. This followed through to calculations on a 6D model of salicylaldimine using MCTDH, but the computational effort required means that convergence of the potential in terms of the number of Gaussians becomes a major difficulty, leading to inaccuracies in the dynamics.

The computational effort required is even greater when calculating electronic energies "on-the-fly" using an electronic structure package. However, the results from these calculations are very promising, with good agreement to the DD-vMCG results of Polyak *et al.* We have thus shown that it is possible to perform MCTDH-based quantum dynamics calculations without the need to pre-compute the PES.

Future work will focus on reducing the computational resources needed to perform MCTDH/GPR calculations on systems with more than a few degrees-of-freedom. Potential ideas to be investigated include the use of an additive kernel for the GPR, where, instead of using a sum of f-dimensional Gaussians as in Eq. (12), each term is a sum of lower dimensional Gaussian functions,[70] potentially leading to efficiencies in evaluating PES matrix elements. It is also possible to include PES gradient information in GPR, and this may offer another route to minimising computational effort, however, it remains to. be seen whether the increased effort in calculating energy gradients counteracts any gains made. Another possible development which we are exploring is to take the GPR representation and use it as a basis for generating a more compact representation of the PES in the style of the well-known high-dimensional model representation (HDMR) strategy.[86,87]

As noted in the Introduction, we have already implemented the method outlined here for multiple electronic states, so it is clear that, if improved efficiency can be achieved, the proposed method has the potential to be of great utility to those wishing to carry out quantum dynamics calculations on a wide selection of molecular systems.

Acknowledgements

We are grateful to the Leverhulme Trust for funding (RPG-2016-055), and to the Scientific Computing Research Technology Platform at the University of Warwick for providing computational resources. The data from Figs. 2-5 can be found at http://wrap.warwick.ac.uk/id/eprint/88404.

References

(1) Boekelheide, N.; Salomón-Ferrer, R.; Miller III, T. F. Dynamics and dissipation in enzyme catalysis. *Proc. Nat. Acad. Sci. USA* **2011**, *108*, 16159–16163.

(2) Masgrau, L.; Roujeinikova, A.; Johannissen, L. O.; Hothi, P.; Basran, J.; Ranaghan, K. E.; Mulholland, A. J.; Sutcliffe, M. J.; Scrutton, N. S.; Leys, D. Atomic Description of an Enzyme Reaction Dominated by Proton Tunneling. *Science* **2006**, *312*, 237–241.

(3) Middleton, C. T.; de La Harpe, K.; Su, C.; Law, Y. K.; Crespo-Hernández, C. E.; Kohler, B. DNA excited-state dynamics: from single bases to the double helix. *Annu. Rev. Phys. Chem.* **2009**, *60*, 217–239.

(4) Stavros, V. G.; Verlet, J. R. Gas-Phase Femtosecond Particle Spectroscopy: A Bottom-Up Approach to Nucleotide Dynamics. *Annual Review of Physical Chemistry* **2016**, *67*, 211–232.

(5) Baker, L. A.; Horbury, M. D.; Greenough, S. E.; Allais, F.; Walsh, P. S.; Habershon, S.; Stavros, V. G. Ultrafast Photoprotecting Sunscreens in Natural Plants. *J. Phys. Chem. Letters* **2016**, *7*, 56–61.

(6) Baker, L. A.; Greenough, S. E.; Stavros, V. G. A Perspective on the Ultrafast Photochemistry of Solution-Phase Sunscreen Molecules. *The Journal of Physical Chemistry Letters* **2016**, *7*, 4655–4665.

(7) Beck, M. H.; Jäckle, A.; Worth, G. A.; Meyer, H. D. The multiconfiguration time-dependent Hartree (MCTDH) method: A highly efficient algorithm for propagating wavepackets. *Phys. Rep.* **2000**, *324*, 1–105.

(8) Schröder, M.; Gatti, F.; Meyer, H.-D. Theoretical studies of the tunneling splitting of malonaldehyde using the multiconfiguration time-dependent Hartree approach. *J. Chem. Phys.* **2011**, *134*, 234307/1–9.

(9) Schröder, M.; Meyer, H.-D. Calculation of the vibrational excited states of malonaldehyde and their tunneling splittings with the multi-configuration time-dependent Hartree method. *J. Chem. Phys.* **2014**, *141*, 034116/1–13.

(10) Coutino-Neto, M.; Viel, A.; Manthe, U. The ground state tunneling splitting of malonaldehyde: Accurate full dimensionl quantum dynamics calculations. *J. Chem. Phys.* **2004**, *121*, 9207–9210.

(11) Neville, S.; Worth, G. A reinterpretation of the electronic spectrum of pyrrole: A quantum dynamics study. *J. Chem. Phys.* **2014**, *140*, 034317/1–13.

(12) Giri, K.; Chapman, E.; Sanz, C. S.; Worth, G. A full-dimensional coupled-surface study of the photodissociation dynamics of ammonia using the multiconfiguration time-dependent Hartree method . *J. Chem. Phys.* **2011**, *135*, 044311/1–13.

(13) Sadri, K.; Lauvergnat, D.; Gatti, F.; Meyer, H.-D. Rovibrational spectroscopy using a kinetic energy operator in Eckart frame and the multi-configuration time-dependent Hartree (MCTDH) approach. *J. Chem. Phys.* **2014**, *141*, 114101/1–11.

(14) Wang, H.; Thoss, M. Multilayer formulation of the multiconfiguration time-dependent Hartree theory. *J. Chem. Phys.* **2003**, *119*, 1289–1299.

(15) Wang, H. Multilayer Multiconfiguration Time-Dependent Hartree Theory. *J. Phys. Chem. A* **2015**, *119*, 7951–7965.

(16) Vendrell, O.; Meyer, H.-D. Multilayer multiconfiguration time-dependent Hartree method: Implementation and applications to a Henon-Heiles Hamiltonian and to pyrazine. *J. Chem. Phys.* **2011**, *134*, 044135/1–16.

(17) Hammer, T.; Manthe, U. Intramolecular proton trnasfer in malonaldehyde: Accurate multilayer multi-configurational time-dependent Hartree calculations. *J. Chem. Phys.* **2011**, *134*, 224305/1–11.

(18) Manthe, U. The multi-configuration time-dependent Hartree approach revisited. *J. Chem. Phys.* **2015**, *142*, 244109/1–15.

(19) Köppel, H.; Domcke, W.; Cederbaum, L. S. Multimode molecular Dynamics beyond the Born-Oppenheimer approximation. *Adv. Chem. Phys.* **1984**, *57*, 59–246.

(20) Cederbaum, L. S.; Köppel, H.; Domcke, W. Multimode vibronic coupling effects in molecules. *Int. J. Quant. Chem.* **1981**, *15*, 251–267.

(21) Meyer, H.-D., Gatti, F., Worth, G. A., Eds. *Multidimensional quantum dynamics: MCTDH theory and applications*; Wiley: Weinheim, Germany, 2009.

(22) Persico, M.; Granucci, G. An overview of nonadiabatic dynamics simulation methods, with focus on the direct approach versus the fitting of potential energy surfaces. *Theo. Chem. Acc.* **2014**, *133*, 1526/1–28.

(23) Worth, G. A.; Robb, M. A.; Lasorne, B. Solving the time-dependent Schrödinger Equation in one step: Direct Dynamics of Non-adiabatic Systems. *Mol. Phys.* **2008**, *106*, 2077–2091.

(24) Tully, J. C.; Preston, R. K. Trajectory surface hopping approach to nonadiabatic molecular collisions: The reaction of H^+ with D_2. *J. Chem. Phys.* **1971**, *55*, 562–572.

(25) Tully, J. C. Molecular dynamics with electronic transitions. *J. Chem. Phys.* **1990**, *93*, 1061–1071.

(26) Richter, M.; Marquetand, P.; González-Vázquez, J.; Sola, I.; González, L. Femtosecond Intersystem Crossing in the DNA Nucleobase Cytosine. *J. Phys. Chem. Lett.* **2012**, *3*, 3090–3095.

(27) Richter, M.; Marquetand, P.; González-Vázquez, J.; Sola, I.; González, L. SHARC: ab Initio Molecular Dynamics with Surface Hopping in the Adiabatic Representation Including Arbitrary Couplings . *J. Chem. Theory Comput.* **2011**, *7*, 1253–1258.

(28) Tully, J. C. Mixed quantum-classical dynamics. *Farad. Discuss.* **1998**, *110*, 407–419.

(29) Coker, D. F. Computer Simulation Methods for Nonadiabatic Dynamics in Condensed Systems. Computer Simulation in Chemical Physics. Dordrecht, 1993; pp 315–377.

(30) Coker, D. F.; Xiao, L. Methods for molecular dynamics with nonadiabatic transitions. *J. Chem. Phys.* **1995**, *102*, 496–510.

(31) Topaler, M. S.; Hack, M. D.; Allison, T. C.; Liu, Y.-P.; Mielke, S. L.; Schwenke, D. W.; Truhlar, D. G. Validation of trajectory surface hopping methods against accurate quantum mechanical dynamics and semiclassical analysis of electronic-to-vibrational energy transfer. *J. Chem. Phys.* **1997**, *106*, 8699–8709.

(32) Hack, M. D.; Truhlar, D. G. Nonadiabatic Trajectories at an Exhibition. *J. Phys. Chem. A* **2000**, *104*, 7917–7926.

(33) Worth, G. A.; Robb, M. A. Applying direct molecular dynamics to non-adiabatic systems. *Adv. Chem. Phys.* **2002**, *124*, 355–432.

(34) Worth, G.; Hunt, P.; Robb, M. Non-adiabatic dynamics: A comparison of surface hopping direct dynamics with quantum wavepacket calculations. *J. Phys. Chem. A* **2003**, *107*, 621–631.

(35) Smith, B. R.; Bearpark, M. J.; Robb, M. A.; Bernardi, F.; Olivucci, M. 'Classical

wavepacket' dynamics through a conical intersection. Application to the S_1/S_0 photochemistry of benzene. *Chem. Phys. Lett.* **1995**, *242*, 27–32.

(36) Bearpark, M. J.; Bernardi, F.; Olivucci, M.; Robb, M. A.; Smith, B. R. Can fulvene S_1 decay be controlled? A CASSCF study with MMVB dynamics. *J. Am. Chem. Soc.* **1996**, *118*, 5254–5260.

(37) Bearpark, M. J.; Bernardi, F.; Clifford, S.; Olivucci, M.; Robb, M. A.; Smith, B. R.; Vreven, T. The azulene S_1 state decays via a conical intersection: A CASSCF study with MMVB dynamics. *J. Am. Chem. Soc.* **1996**, *118*, 169–175.

(38) Mitrić, R.; Petersen, J.; Bonacić-Koutecký, V. Laser-field-induced surface-hopping method for the simulation and control of ultrafast photodynamics. **2009**, *79*, 053416/1–6.

(39) Mitrić, R.; Petersen, J.; Wohlgemuth, M.; Werner, U.; Bonacić-Koutecký, V. Field-induced surface hopping method for probing transition state nonadiabatic dynamics of Ag3. *Phys. Chem. Chem. Phys.* **2011**, *13*, 8690–8696.

(40) Mitrić, R.; Petersen, J.; Wohlgemuth, M.; Werner, U.; Bonacić-Koutecký, V.; Wöste, L.; Jortner, J. Time-Resolved Femtosecond Photoelectron Spectroscopy by Field-Induced Surface Hopping. *J. Phys. Chem. A* **2011**, *115*, 3755–3765.

(41) Lisinetskaya, P.; Mitrić, R. Simulation of laser-induced coupled electron-nuclear dynamics and time-resolved harmonic spectra in complex systems. **2011**, *83*, 033408/1–13.

(42) Hack, M. D.; Jasper, A.; Volobuev, Y. L.; Schwenke, D. W.; Truhlar, D. G. Quantum Mechanical and Quasiclassical Trajectory Surface Hopping Studies of the Electronically Nonadiabatic Predissociation of the $\tilde{A}$ State of NaH_2. *J. Phys. Chem. A* **1999**, *103*, 6309–6326.

(43) Ben-Nun, M.; Quenneville, J.; Martínez, T. J. Ab initio multiple spawning: photochemistry from first principles quantum molecular dynamics. *J. Phys. Chem. A* **2000**, *104*, 5161–5175.

(44) Ben-Nun, M.; Martínez, T. J. *Ab Initio* Quantum Molecular Dynamics. *Adv. Chem. Phys.* **2002**, *121*, 439–512.

(45) Hudock, H. R.; Levine, B. G.; Thompson, A. L.; Satzger, H.; Townsend, D.; Gador, N.; Ullrich, S.; Stolow, A.; Martínez, T. J. Ab initio molecular dynamics and time-resolved photoelectron spectroscopy of electronically excited uracil and thymine. *J. Phys. Chem. A* **2007**, *111*, 8500–8508.

(46) Mori, T.; Glover, W.; Schuurman, M.; Martínez, T. Role of Rydberg States in the Photochemical Dynamics of Ethylene. *J. Phys. Chem. A* **2012**, *116*, 2808–2818.

(47) Ko, C.; Levine, B.; Toniolo, A.; Manohar, L.; Olsen, S.; Werner, H.-J.; Martínez, T. J. Ab initio excited-state dynamics of the photoactive yellow protein chromophore. *J. Am. Chem. Soc.* **2003**, *125*, 12710–12711.

(48) Worth, G.; Burghardt, I. Full quantum mechanical molecular dynamics using Gaussian wavepackets. *Chem. Phys. Lett.* **2003**, *368*, 502–508.

(49) Burghardt, I.; Meyer, H.-D.; Cederbaum, L. S. Approaches to the approximate treatment of complex molecular systems by the multiconfiguration time-dependent Hartree method. *J. Chem. Phys.* **1999**, *111*, 2927–2939.

(50) Richings, G.; Polyak, I.; Spinlove, K.; Worth, G.; Burghardt, I.; Lasorne, B. Quantum Dynamics Simulations using Gaussian Wavepacket: The vMCG Method. *Int. Rev. Phys. Chem.* **2015**, *34*, 269–308.

(51) Worth, G. A.; Robb, M. A.; Burghardt, I. Non-adiabatic Direct Dynamics using Vari-

ational Gaussian Wavepackets: The $\tilde{X}/\tilde{A}$ Manifold of the Butatriene Cation. *Farad. Discuss.* **2004**, *127*, 307–323.

(52) Lasorne, B.; Sicilia, F.; Bearpark, M. J.; Robb, M. A.; Worth, G. A.; Blancafort, L. Automatic generation of active coordinates for quantum dynamics calculations: Application to the dynamics of benzene photochemistry. *J. Chem. Phys.* **2008**, *128*, 124307/1–10.

(53) Lasorne, B.; Bearpark, M. J.; Robb, M. A.; Worth, G. A. Controlling S1/S0 Decay and the Balance between Photochemistry and Photostability in Benzene: A Direct Quantum Dynamics Study . *J. Phys. Chem. A* **2008**, *112*, 13017–13027.

(54) Lasorne, B.; Robb, M. A.; Worth, G. A. Direct quantum dynamics using variational multi-configuration Gaussian wavepackets. Implementation details and test case. *Phys. Chem. Chem. Phys.* **2007**, *9*, 3210–3227.

(55) Mendive-Tapia, D.; Lasorne, B.; Worth, G.; Bearpark, M.; Robb, M. Controlling the mechanism of fulvene S1/S0 decay: switching off the stepwise population transfer. *Phys. Chem. Chem. Phys.* **2010**, *12*, 15725–15733.

(56) Mendive-Tapia, D.; Lasorne, B.; Worth, G.; Robb, M.; Bearpark, M. Towards converging non-adiabatic direct dynamics calculations using frozen-width variational Gaussian product basis functions . *J. Chem. Phys.* **2012**, *137*, 22A548/1–10.

(57) Allan, C.; Lasorne, B.; Worth, G.; Robb, M. A Straightforward Method of Analysis for Direct Quantum Dynamics: Application to the Photochemistry of a Model Cyanine. *J. Phys. Chem. A* **2010**, *114*, 8713–8729.

(58) Asturiol, D.; Lasorne, B.; Worth, G.; Bearpark, M.; Robb, M. Exploring the sloped-to-peaked S2/S1 seam of intersection of thymine with electronic structure and direct quantum dynamics calculations. *Phys. Chem. Chem. Phys.* **2010**, *12*, 4949–4958.

(59) Araújo, M.; Lasorne, B.; Magalhaes, A.; Bearpark, M.; Robb, M. Controlling Product Selection in the Photodissociation of Formaldehyde: Direct Quantum Dynamics from the S1 Barrier. *J. Phys. Chem. A* **2010**, *114*, 12016–12020.

(60) Polyak, I.; Allan, C.; Worth, G. A complete description of tunnelling using direct quantum dynamics simulation: Salicylaldimine proton transfer. *J. Chem. Phys.* **2015**, *143*, 084121/1–10.

(61) Araújo, M.; Lasorne, B.; Magalhaes, A.; Worth, G.; Bearpark, M.; Robb, M. The molecular dissociation of formaldehyde at medium photoexcitation energies: A quantum chemistry and direct quantum dynamics study. *J. Chem. Phys.* **2009**, *131*, 144301/1–8.

(62) Vacher, M.; Bearpark, M. J.; Robb, M. A. Direct methods for non-adiabatic dynamics: connecting the single-set variational multi-configuration Gaussian (vMCG) and Ehrenfest perspectives. *Theor. Chem. Acc.* **2016**, *135*, 187/1–11.

(63) Habershon, S. Linear dependence and energy conservation in Gaussian wavepacket basis sets. *J. Chem. Phys.* **2012**, *136*, 014109/1–8.

(64) Rasmussen, C. E.; Williams, C. K. *Gaussian Processes for Machine Learning*; The MIT Press: Cambridge, Massachusetts, 2006.

(65) Williams, C. In *Handbook of Brain Theory and Neural Networks*; Arbib, M., Ed.; The MIT Press: Cambridge, Massachusetts, 2002; pp 466–470.

(66) Bartók, A.; Csányi, G. Gaussian Approximation Potentials: A Brief Tutorial Introduction. *Int. J. Quantum. Chem.* **2015**, *115*, 1051–1057.

(67) Alborzpour, J. P.; Tew, D. P.; Habershon, S. Efficient and accurate evaluation of potential energy matrix elements for quantum dynamics using Gaussian process regression. *J. Chem. Phys.* **2016**, *145*, 174112/1–11.

(68) Mones, L.; Bernstein, N.; Csányi, G. Exploration, Sampling, And Reconstruction of Free Energy Surfaces with Gaussian Process Regression. *J. Chem. Theory Comput.* **2016**, *12*, 5100–5110.

(69) Quinonero-Candela, J.; Ramussen, C. E.; Williams, C. K. I. In *Large-Scale Kernel Machines*; Bottou, L., Chapelle, O., DeCoste, D., Weston, J., Eds.; The MIT Press: Cambridge, Massachusetts, 2007; pp 203–224.

(70) Duvenaud, D.; Nickisch, H.; Rasmussen, C. E. Additive Gaussian Processes. Neural Information Processing Systems Conference. 2011.

(71) Chalupka, K.; Williams, C. K.; Murray, I. A Framework for Evaluating Approximation Methods for Gaussian Process Regression. *J. Mach. Learn Res.* **2013**, *14*, 333–350.

(72) Mizukami, W.; Habershon, S.; Tew, D. A compact and accurate semi-global potential energy surface for malonaldehyde from constrined least squares regression. *J. Chem. Phys.* **2014**, *141*, 144310/1–9.

(73) Meyer, R.; Ha, T.-K. Quantum states of hydrogen transfer and vibration in malonaldehyde. *Mol. Phys.* **2003**, *101*, 3263–3276.

(74) Cvitaš, M. T.; Althorpe, S. C. Locating Instantons in Calculations of Tunneling Splittings: The Test Case of Malonaldehyde. *J. Chem. Theory Comput.* **2016**, *12*, 787–803.

(75) Wu, F.; Ren, Y.; Bian, W. The hydrogen tunneling splitting in malonaldehyde: A full-dimensional time-independent quantum mechanical method. *J. Chem. Phys.* **2016**, *145*, 074309/1–9.

(76) Petković, M.; Kühn, O. Multidimensional Hydrogen Bond Dynamics in Salicylaldimine: Coherent Nuclear Wave Packet Motion versus Intramolecular Vibrational Energy Redistribution. *J. Phys. Chem. A* **2003**, *107*, 8458–8466.

(77) Richings, G.; Habershon, S. *Chem. Phys. Lett.* **2017**, In press, DOI: 10.1016/j.cplett.2017.01.063.

(78) Tannor, D. J. *Introduction to Quantum Mechanics A Time-Dependent Perspective*; University Science Books: Sausalito, California, 2007.

(79) Dirac, P. Note on Exchange phenomena in the Thomas atom. *Proc. Cambridge Philos. Soc.* **1930**, *26*, 376–385.

(80) Frenkel, J. *Wave Mechanics*; Clarendon Press, Oxford, 1934.

(81) Worth, G.; Giri, K.; Richings, G.; Burghardt, I.; Beck, M.; Jäckle, A.; Meyer, H.-D. *The Quantics Package, Version 1.1*; 2016.

(82) Anderson, E.; Bai, Z.; Bischof, C.; Blackford, S.; Demmel, J.; Dongarra, J.; Du Croz, J.; Greenbaum, A.; Hammarling, S.; McKenney, A.; Sorensen, D. *LAPACK Users' Guide*, 3rd ed.; Society for Industrial and Applied Mathematics: Philadelphia, PA, 1999.

(83) Ischtwan, J.; Collins, M. A. Molecular potential energy surfaces by interpolation. *J. Chem. Phys.* **1994**, *100*, 8080–8088.

(84) Collins, M. A.; Zhang, D. H. Application of interpolated potential energy surfaces to quantum reactive scattering. *J. Chem. Phys.* **1999**, *111*, 9924–9931.

(85) Neese, F. The ORCA Program System. *Wiley Interdiscip. Rev: Comput. Mol. Sci.* **2012**, *2*, 73–78.

(86) Ho, T.-S.; Rabitz, H. Reproducing kernel Hilbert space interpolation methods as a paradigm of high dimensional model representations: Application to multidimensional potential energy construction. *J. Chem. Phys.* **2003**, *119*, 6433–6442.

(87) Aliş, O.; Rabitz, H. Efficient implementation of high dimensional model representations. *J. Math. Chem.* **2001**, *29*, 127–142.